



Masayasu Ohtsu and Dimitrios G. Aggelis

Abstract Physically, fracture in a material takes place as the release of stored strain energy, which is consumed by nucleating new external surfaces (cracks) and emitting elastic waves. The elastic waves propagate inside the material and are detected by an acoustic emission (AE) sensor. In this concern, important aspects are to select proper sensors and instrumental systems. Depending upon materials and structures, selection of sensors, decision of frequency range, techniques to eliminate noises and conditions for system setting are to be taken carefully into account. Consequently, standardized procedures and requirements for systems are stated. They include the system response based on the linear-system theory, response of PZT element as a contact-type sensor, mounting of sensors and its aperture effect, instrumental bases and data acquisition.

Keywords Linear-system theory · PZT element · Resonant frequency · Calibration · Sensor coupling, · Aperture effect

1 Introduction

From the physical viewpoint, fracture in a material takes place as the release of stored strain energy, which is consumed by nucleating new external surfaces (cracks) and emitting elastic waves. The latter is defined as AE phenomenon. The elastic waves propagate inside the material and are detected by an AE sensor. Except for contactless sensors, AE sensors are directly attached on the surface as shown in Fig. 1.

M. Ohtsu (✉)

Graduate School of Engineering, Kyoto University, Kyoto 615-8540, Japan
e-mail: Ohtsu.masayasu.4v@kyoto-u.ac.jp

D. G. Aggelis

Department of Mechanics of Materials and Constructions, Vrije Universiteit Brussel, 1050 Brussels, Belgium
e-mail: Dimitrios.aggelis@vub.be

© Springer Nature Switzerland AG 2022

C. U. Grosse et al. (eds.), *Acoustic Emission Testing*, Springer Tracts in Civil Engineering, https://doi.org/10.1007/978-3-030-67936-1_3

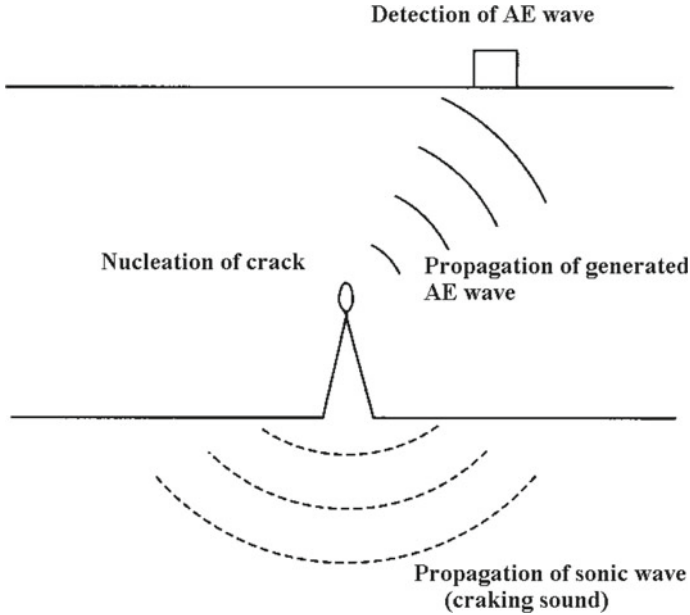


Fig. 1 Detection of AE wave

A contact type of the sensor is normally employed in AE measurement, and is commercially available. In the most cases, a piezoelectric element in a protective housing (Beattie 1983) as illustrated in Fig. 2 is applied to detection. These sensors are exclusively based on the piezoelectric effect out of lead zirconate titanate (PZT).

For a specialized purpose of sensor calibration, a capacitive sensor (transducer) is developed (Breckenridge 1982). Compared with other types of AE sensors, it is well known that piezoelectric sensors provide the best combination of low cost, high sensitivity, ease of handling and selective frequency responses. Although PZT sensors are not normally suited for broad-band detection in basic studies of AE waveform analysis, they are practically useful for most AE experiments and applications.

2 Sensor and System Response

AE signals are detected, as dynamic motions at the surface of a material, and are converted into electric signals. Then the electrical signals are amplified and filtered. Mathematically, the system response is formulated by a linear system in Fig. 3. Here, input function $f(t)$ of the surface motion is transformed into function $g(t)$ of the electric signal by transfer function $L[]$ of AE sensor. This system is mathematically formulated as,

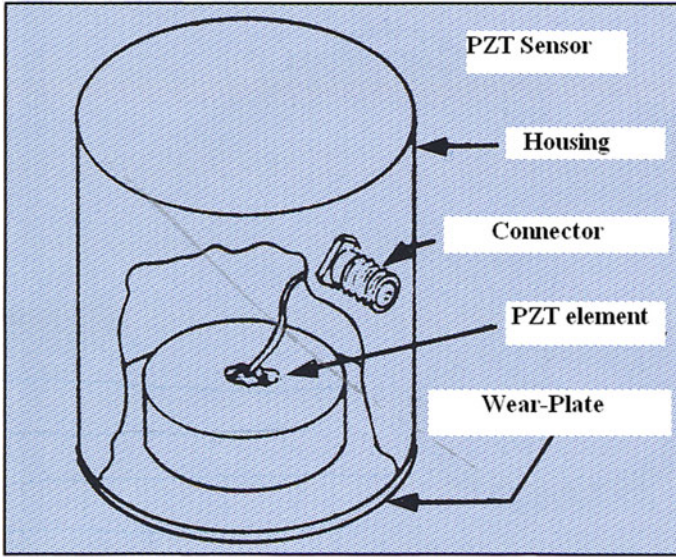
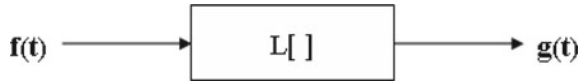


Fig. 2 AE sensor of the piezoelectric element

Fig. 3 A linear system



$$g(t) = L[f(t)]. \tag{1}$$

Here, the convolution integral $s(t)$ is defined as an integration of two functions $f(t)$ and $w(t)$,

$$s(t) = \int f(t - \tau)w(\tau)d\tau = f(t) * w(t). \tag{2}$$

The symbol $*$ represents the convolution. Then Dirac’s delta function $\delta(t)$ plays an important role. By definition, it can be expressed as,

$$f(t) = f(t) * \delta(t). \tag{3}$$

In the case of a linear system, Eq. 1 becomes,

$$g(t) = L[f(t) * \delta(t)] = f(t) * L[\delta(t)].$$

Setting $L[\delta(t)]$ as $w(t)$, we have,

$$g(t) = f(t) * w(t). \tag{4}$$

This implies that the sensor response $g(t)$ is obtained from the convolution of the input, $f(t)$, with the impulse response of the system, $w(t)$, because the function $L[\delta(t)]$ is the response of the system due to the input of the delta function. Introducing the Fourier transform,

$$G(f) = \int g(t) \exp(-j2\pi ft) dt = \int \int f(t - \tau) w(\tau) d\tau \exp(-j2\pi ft) dt,$$

and setting $t - \tau = s$, we have

$$\begin{aligned} G(f) &= \int f(s) \exp(-j2\pi fs) ds \int w(t) \exp(-j2\pi ft) dt \\ &= F(f)W(f). \end{aligned} \quad (5)$$

Here $G(f)$, $F(f)$ and $W(f)$ are Fourier transforms of $g(t)$, $f(t)$ and $w(t)$, respectively. $W(f)$ is often named the transfer function and the function of frequency response of the sensor. Thus, a calibration of AE sensor is equivalent to determination of function $W(f)$. On the other hand, it implies that frequency contents of AE waves are usually smeared by function $w(t)$ of AE sensor. Thus, the absolute calibration means quantitative estimation of function $w(t)$ or $W(f)$.

The signals measured using AE sensor are of small magnitude compared to other methods. As a result, AE signals obtained by the sensors are very weak and must be amplified to be detected and recorded. The influence of amplification and possible filtering can be assigned with different transfer functions. Consequently, an AE signal $a(t)$ recorded in the system illustrated in Fig. 2.8 is mathematically represented as,

$$a(t) = w_f(t) * w_a(t) * w(t) * f(t), \quad (6)$$

where $w_f(t)$ and $w_a(t)$ are transfer functions of the filter and the amplifiers. For characterizing AE sources theoretically, it is important to know the weights of these functions as to quantify their influences. In usual cases, the transfer functions of both the filter $w_f(t)$ and the amplifier $w_a(t)$ are known to be fairly flat or almost constant in the frequency domain. As a result, it is found that the frequency response or the transfer function $w(t)$ or $W(f)$ of AE sensor dominantly affects the frequency contents of AE signals. Theoretically, the time function of the source is relatively simple, since it originates by a single step-function motion of a crack propagation increment that takes place in a time period of possibly ns. Except for source kinematics, experimentally this can be simulated by glass capillary tube break, ball impact or pencil lead break (McLaskey and Glaser 2012). However, the physics of wave propagation and transduction are extremely complicated. Therefore, the waveform recorded by the sensor becomes much longer and more complex due to the contribution of the above-mentioned transfer functions, as indicatively shown in Fig. 4.

Maintaining a constant setup enables comparisons between different sources, but it should always be kept in mind that the final, recorded signal and its characteristics

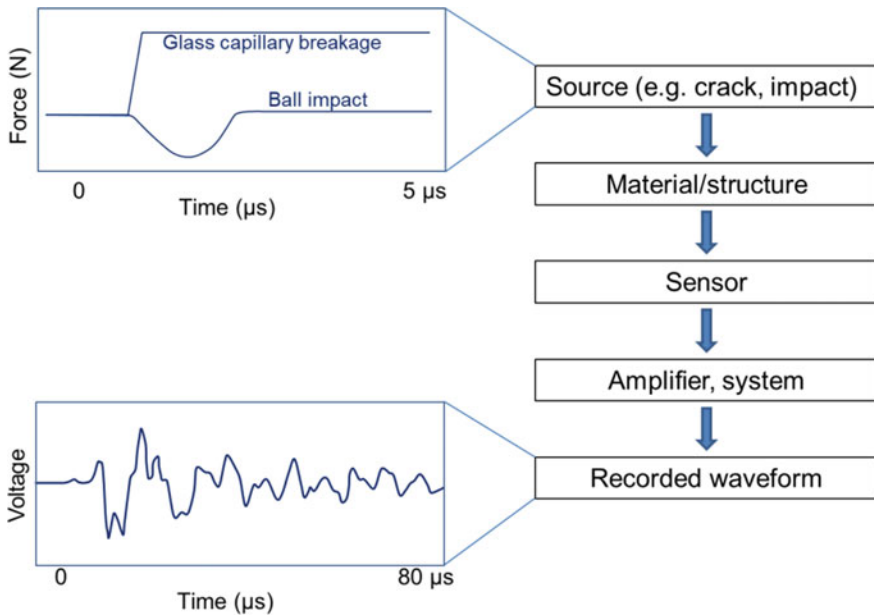


Fig. 4 Process chain of AE and indicative excitations (top) and received waveform (bottom). (Similar to McLaskey and Glaser 2012)

are not necessarily close to the ones of the original source, especially in the case of resonant sensors.

3 Response of PZT Sensor

In the case of piezoelectric or PZT sensors, the sensors are usually operated in resonance, i.e. the signals are recorded in a small frequency range due to the frequency characteristics of the sensor to enhance the detection of AE signals. Very damped sensors are operated outside their resonance frequencies allowing a broadband detection, although they are usually less sensitive to wave motions than the resonance type.

So far various analyses of PZT sensors have been performed. These can be classified into two groups. One employed equivalent electric circuit (Mason 1958) and the other applied solutions of the field equations (Auld 1973). These are based on one-dimensional analysis, and thus results can not be readily extended to three-dimensional (3-D) analysis. This is because the PZT element used in AE sensor is neither an infinite bar nor an infinite plate.

A few solutions exist for 3-D PZT bodies. Most well-known solutions for finite PZT plates were obtained from approximated two-dimensional (2-D) equations of

extended Mindlin's solutions (Herrmann 1974). However, these solutions are not directly applicable to the analysis of commercially available AE sensors. In order to clarify the frequency response of AE sensor (function $W(f)$ in Eq. 5) and to optimize the design of PZT elements, resonance characteristics of PZT element were analyzed by using the finite element method (FEM) (Ohtsu and Ono 1983).

Electro-mechanical vibrations of PZT bodies can be solved in a manner similar to the corresponding mechanical vibration problem, but with additional variables. The constitutive laws of PZT materials are represented, as follows (Holland and EerNisse 1969; Kawabata 1973),

$$\{\varepsilon\} = [C]\{\sigma\} + [d]^T\{E\}, \quad (7)$$

$$\{D\} = [d]\{\sigma\} + [p]\{E\}. \quad (8)$$

Here $\{\varepsilon\}$ are the elastic strains, $\{E\}$ are the stresses, $\{E\}$ are the electric potentials and $\{D\}$ are the electric displacements. $[C]$ represents the adiabatic elastic compliance tensor at constant electric field, $[d]$ is the adiabatic piezoelectric tensor and $[p]$ is the adiabatic electric permittivity at constant stress. From these constitutive equations, it is readily known that the piezoelectric element generates electric signals due to mechanical motions and vice versa.

As analytical results, three PZT-5A elements were analyzed by the FEM, of which material properties were known. These are a cylindrical element of 9.53 mm diameter and 12.19 mm height, a disk-shaped element of 9.53 mm diameter and 1.45 mm height, and a truncated conical element of 6 mm base-diameter, 1 mm truncated end-diameter and 2.5 mm height. From piezoelectric constants in Eqs. 7 and 8, nominal resonance frequencies of such fundamental modes as compression, shear and radial can be calculated in the cases of the cylindrical and the disk-shaped elements. The results are given in Table 1.

In the FEM analysis, axi-symmetric models are analyzed. In order to investigate the coupling effect between the sensor and the medium, two cases of stress-free boundary (free vibration) and fixed boundary at the contact surface are analyzed to determine resonant frequencies and modes.

In Table 1, resonant frequencies obtained experimentally are compared to nominal resonances. In the cases of the cylindrical and disk-shaped elements, the resonant frequencies are obtained as in reasonable agreement with nominal resonances of the shear and the radial for free vibration, while the nominal resonance of the compression seems to be analyzed for fixed boundary.

Resonant vibration modes of the conical element for the case of free vibration and of fixed boundary are shown in Fig. 5. To show the vibration modes clearly, scales of displacements are highly exaggerated. In all the cases, simple modes of the vibration envisaged in the nominal modes are not observed. When the bottom boundary is constrained in motions, the resonant frequencies are shifted to the higher mode. In addition, the vibration modes change from a bending mode to a mixture of shear and compression. Thus, the resonant frequencies appear as different modes

Table 1 Resonant frequencies of PZT elements

Shape	Free vibration (kHz)			Fixed boundary (kHz)		
	Nominal	FEM analysis	Experiment	Nominal	FEM analysis	Experiment
Cylindrical element	<u>71 (shear)</u>	<u>109</u>	<u>133</u>	71 (shear)	61	42
	<u>160</u>	196	<u>210</u>	<u>160</u>	<u>167</u>	<u>152</u>
	(comp.)	207	251	(comp.)	191	204
	<u>201</u>	217	312	<u>201</u>	245	
	(radial)	298		(radial)	316	
Disk-shaped element	<u>201</u>	116	42	<u>1343</u>	382	291
	(radial)	206	91	(comp.)	766	516
	<u>597</u>	322	146		1219	720
	(shear)	541	<u>166</u>		<u>1476</u>	
		<u>581</u>	231		2245	
		536				
Conical element		80	66		404	404
		262	278		803	500
		414	494		878	570
		567	713		1099	766
		774			1874	

from the nominal modes, because the PZT element vibrates three-dimensionally. As illustrated in Fig. 2, the PZT element is fixed in a housing case. Therefore, the case of fixed boundary might be of a plausible resonant mode in the sensor.

In order to evaluate the resonant frequencies analyzed, experiments are conducted by employing a block diagram in Fig. 6. For free vibration, a PZT-5A element is placed on a steel block of dimensions 570 mm × 130 mm × 180 mm with grease coupling. Sweeping sinusoidal input from dc to 2 MHz is supplied by a function generator to a broad-band sensor (FC500 model, AET), which is coupled to the same surface of the block as a transmitter in the figure. The input voltage is kept constant during a sweeping time of about 50 s., but it is adjusted to obtain enough output voltage for recording. The output voltage of the PZT-5A element is amplified as 80 dB in total and filtered with the band-pass from 30 kHz to 2 MHz. The root-mean-square (RMS) voltage output is recorded.

In the case of fixed boundary, the PZT-5A element is bonded with wax. Results of the conical element are shown in Fig. 7. In the case of free vibration, more than ten peak frequencies are found from 66 kHz to 2 MHz. The main effect of the steel block is to confine the peak frequencies to the 400–600 kHz range. A strong peak is observed at around 500 kHz both in the free vibration and after bonding to the steel block.

All the major peaks or resonant frequencies obtained are also listed in Table 1. They are compared with the nominal resonances and the resonances by the FEM analysis. Generally, the peak frequencies determined by three different methods are in reasonable agreement. In the case of the nominal resonant frequencies, no boundary conditions are assigned. The values of resonances are listed as corresponding values.

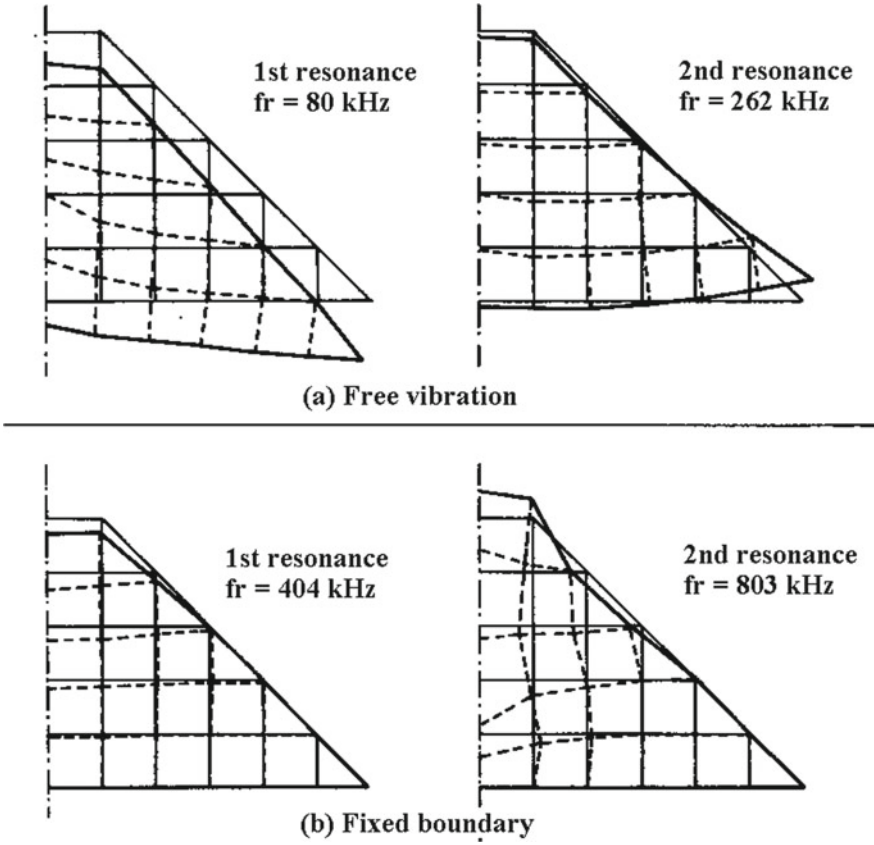


Fig. 5 Resonant vibration modes of the conical element

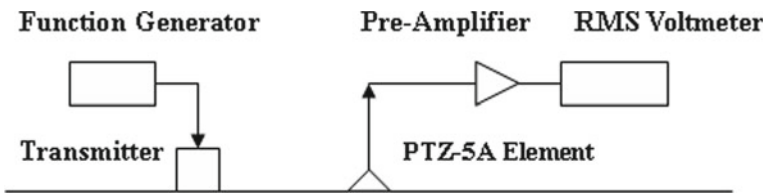


Fig. 6 Experimental set-up for frequency responses of PZT elements

In the cylindrical element, the effect of fixed boundary is minor, because the small area at the bottom is only constraint. It is noted that the resonant frequency lower than the compression mode is obtained in the case of fixed boundary, which is close to the resonance of the shear mode. In the disk-shaped element, lower resonant frequency than that of the radial mode is obtained in both the FEM analysis and the experiment in the case of free vibration. These disappear in the case of fixed boundary, where

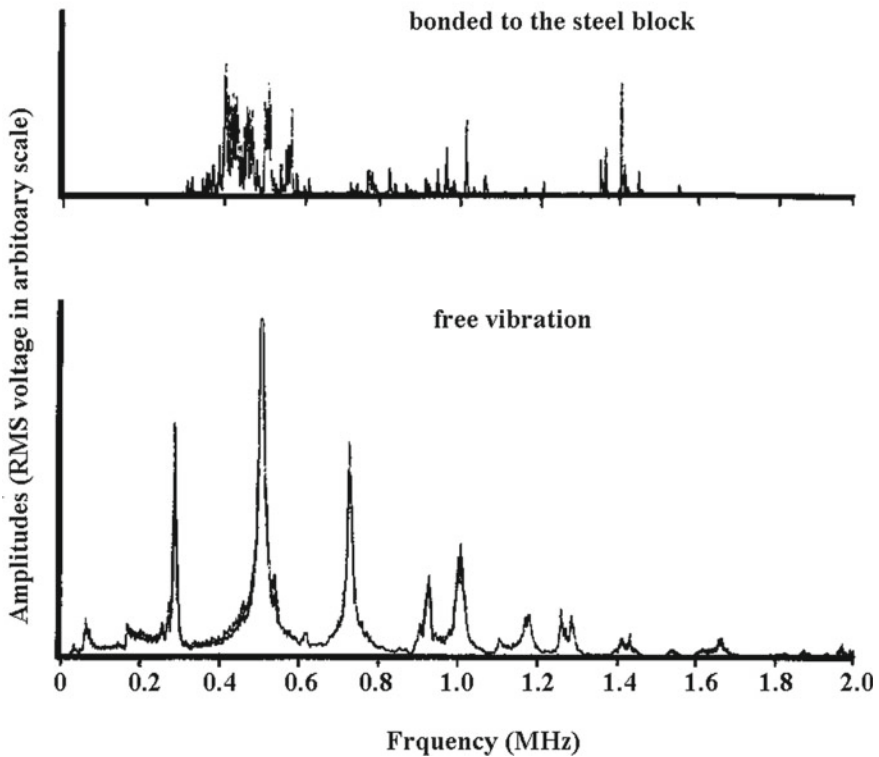


Fig. 7 Frequency responses of the conical element

the resonant frequency corresponds to the compression mode obtained in the FEM analysis. In the conical element, higher resonant frequencies are obtained in the case of fixed boundary. According to Fig. 7, the responses of these resonance frequencies are fairly weak.

A NIST (National Institute for Standards and Technology, U. S. A.) conical transducer (Proctor 1982) has been known as a reference sensor of flat response. Because the sensor consists of a conical element of 1.5 mm truncated-end in diameter bonded to a brass cylinder as illustrated in Fig. 8. Taking into account the frequency spectrum in the bonded case in Fig. 7, it is suggested to have weak peak frequencies in the low frequency range from 100 kHz to 1 MHz as well as low sensitivity.

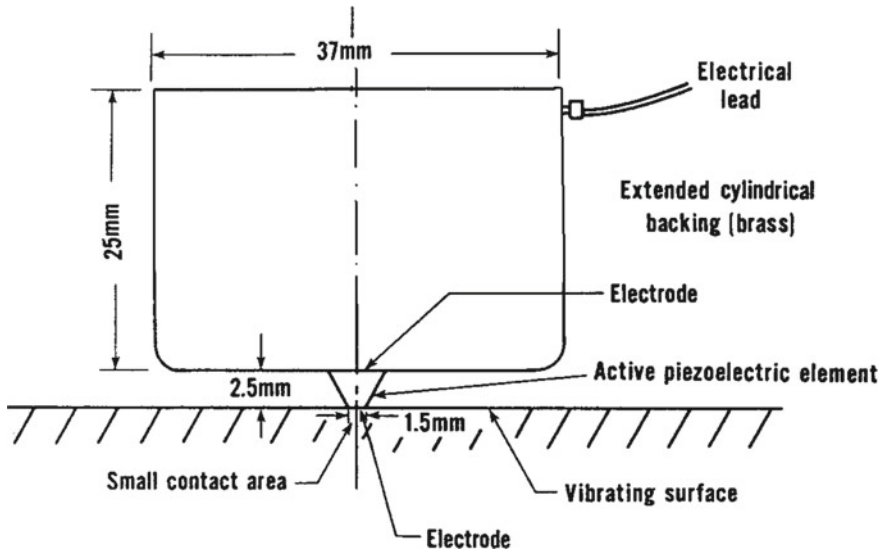


Fig. 8 Sketch of NIST conical transducer

4 Detection by Sensors

A typical AE sensor of PZT element transforms elastic motions of 1 μm displacement into electrical signals of 1 μV voltage. As an example, frequency responses of commercially available AE sensors are given in Fig. 9. The top figure shows the response of a broadband sensor and the bottom is that of a resonance type. Although both sensors respond irregularly, the sensitivity of the broadband type is lower than that of the resonance type. This fact implies that the selection of AE sensors should be based on either the sensitivity (resonance type) or the flat response in the frequency range (broadband type). In any case where AE waves are detected by AE sensor, frequency contents are smeared by the transfer function $W(f)$ of the sensor as discussed in Eq. 6.

As a small parenthesis it is mentioned that when the sensor cannot be attached directly to the structure, waveguides as illustrated in Fig. 10 are mounted between the inspected structure and the sensor. This is usually the case when monitoring at high temperatures (common in ceramic materials) since normal PZT sensors cannot be used at temperatures higher than 200 $^{\circ}\text{C}$, or in general in harmful environments (Godin et al. 2018; Papasalouros et al. 2016). Waveguides certainly impose a significant effect due to their transfer function, in essence they attenuate and distort the frequency contents of AE waves (Zelenyak et al. 2015).

Going back to the responses in Fig. 9 are results calibrated by two methods of the sensor calibration. One is a calibration method by NIST, as illustrated in Fig. 11 (Breckenridge 1982). A large steel block of 90 cm diameter and 43 cm long was employed. As a step-function impulse, a glass capillary source was employed, and

elastic waves were detected by a capacitive transducer and by a sensor under calibration. The calibration curve is to be obtained from the ratio of a frequency spectrum by a tested sensor to that of the capacitive transducer. The capacitive transducer (sensor) could record a Lamb's solution due to surface pulse as discussed in chapter "Source Mechanisms". It is reasonably assumed that the capacitive transducer detects the vertical displacement at the surface due to a step-function force. The other is known as a reciprocity method, which was developed by Hatano and Watanabe (1997) as indicated by broken curves in the figure. A reasonable agreement with the NIST method is reported.

In the absolute calibration proposed by NIST, the capacitive transducer was employed. This is because the transducer could detect displacements motions without unnecessary distortion. Recently, a laser vibrometer is also available as a displacement-meter, although its sensitivity is as low as the capacitive transducer. In the NIST method, a standard source was generated by a capillary break and later by a pencil-lead break (Hsu and Breckenridge 1981) as a step-function. They compared detected displacement motions with Lamb's solution of the surface pulse (Pekeris 1955). A numerical program to compute Lamb's solutions was already published (Ohtsu and Ono 1984). By employing this program, surface motions due to steel-ball drop can be numerically computed. The laser vibrometer is usually applied to detect velocity motions. Therefore, velocity motions of numerical results are compared with those detected by the laser vibrometer, and results are shown in Fig. 12. According to Sansalone and Streett (1997), contact time T_c of steel-ball drop is given by.

$$T_c = 0.0043D, \quad (9)$$

where D is the radius of the steel ball. The time function $S(t)$ of steel-ball drop is assumed as,

$$S(t) = \cos^4\left(\frac{\pi}{2T_c}t - \frac{\pi}{2}\right). \quad (10)$$

In this case, the upper-bound frequency f_c is given by,

$$f_c = 1.25/T_c \quad (11)$$

In Fig. 12, velocity motion detected by the laser vibrometer is shown at the top and that of Lamb's solution is shown at the middle. Remarkable agreement is confirmed except the latter reflections in the detected wave, which are due to the geometry of the concrete block employed in the experiment. At the bottom, a frequency spectrum of the detected wave is shown as a solid curve and is compared with that of Lamb's solution denoted by a dash curve. Reasonable agreement is again confirmed. This result suggests an application of the laser vibrometer for the absolute calibration instead of the capacitive transducer.

As shown in Fig. 9, sensitivity of AE sensor is often expressed in voltage output per vertical velocity (1 V/(m/s)). In another way, the face-to-face technique has been

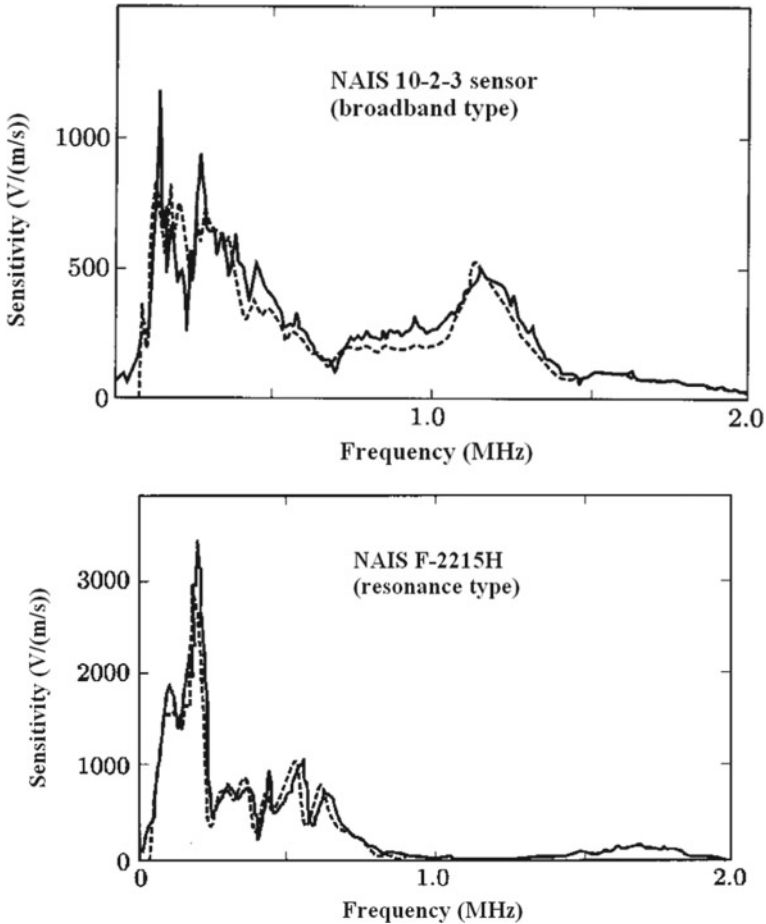


Fig. 9 Calibration curves of frequency responses of commercial AE sensors

conventionally applied to estimate the sensitivity based on voltage output per unit pressure input (1 V/mbar). The broadband sensor is casually used as a reference. Some examples are given in Fig. 13. It must be emphasized that practically the response of resonant AE sensors reaches values of several V per nm of surface displacement, showing the high standards of sensitivity of the technique (To and Glaser 2005).

For the PZT sensors, contactless measurement is an exception in AE measurement. Coupling between sensors and a member is important due to the low amplitudes of AE signals. Therefore, various methods exist for fixing the sensors to the structure. Adhesives or gluey coupling materials and couplants such as wax and grease are often used due to their low impedance. If the structure has a metallic surface, magnetic or immersion techniques are applicable. Other methods using a spring or rapid cement

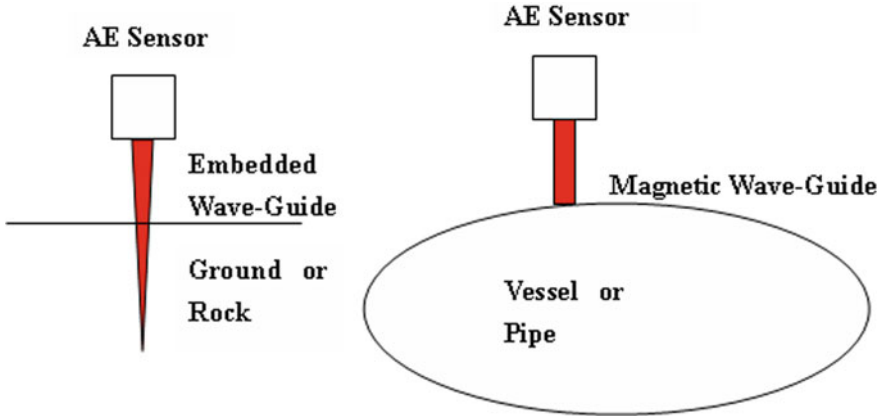
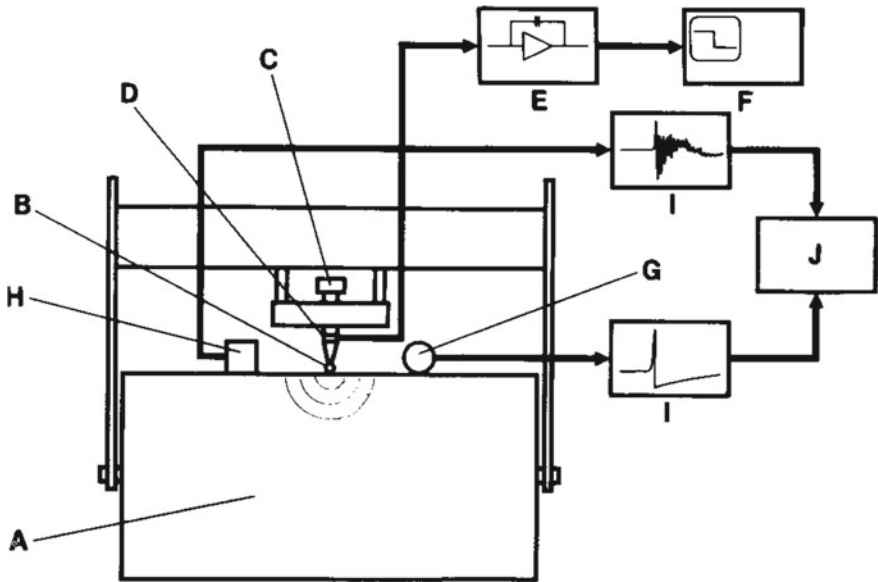


Fig. 10 Examples of AE wave-guides



Schematic diagram of the apparatus: A. steel transfer block; B. capillary source; C. loading screw; D. PZT disc; E. charge amplifier; F. storage oscilloscope; G. standard transducer; H. transducer under test; I. transient recorders; J. computer

Fig. 11 Experimental set-up for the absolute calibration of AE sensor by NIST

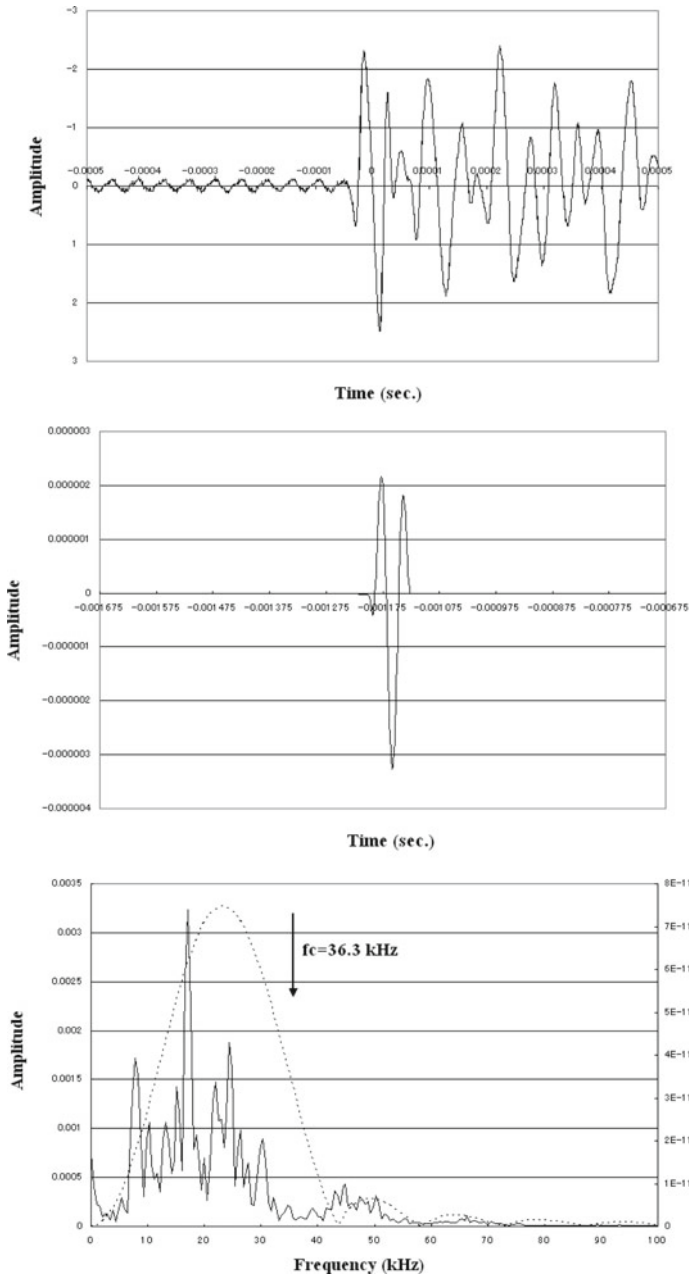


Fig. 12 Velocity motion detected by the laser vibrometer (top), calculated Lamb's solution of velocity motion (middle), and their frequency spectra (bottom). The solid curve comes from the motion detected by the laser vibrometer and the dash curve is the calculated Lamb's solution

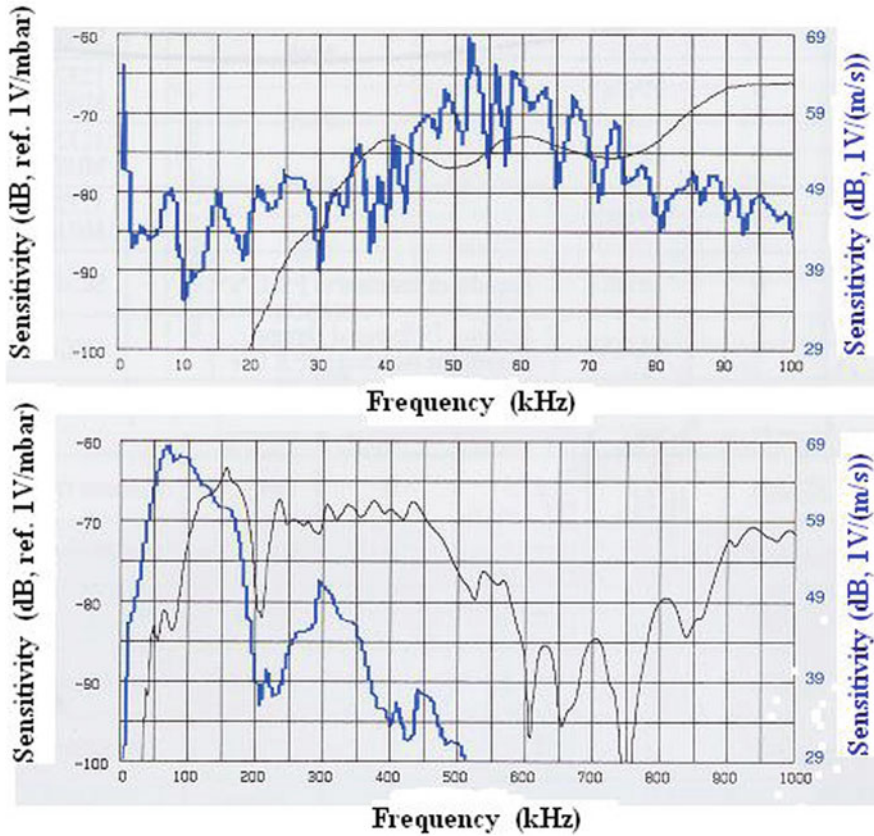


Fig. 13 Calibration curves of AE sensors

can be used. In general, the coupling should reduce the loss of signal energy and should have a low acoustic impedance compared to the material to be tested. To decrease the attenuation of waves, it is necessary to avoid air bubbles and thick glue/couplant layers. An essential requirement in mounting a sensor is sufficient acoustic coupling between the surface of sensors and that of the member to make sure that a contact surface is smooth and clean, allowing for good adhesion. The couplant layer should be thin, but enough to fill gaps caused by surface roughness and eliminate air gaps to ensure good acoustic transmission. Commonly used couplants are vacuum greases, water-soluble glycols, solvent-soluble resins, and proprietary ultrasonic couplants.

In addition to coupling, the sensor must always be stationary. One way to achieve this condition is to use glue, which can also serve as a couplant. Before using a glue, the ease of removal should be taken care of, since not all sensors can withstand a large removal force between the housing and the mounting face (wear plate). Another way to safely mount a sensor is to use holding devices such as tapes, elastic bands,

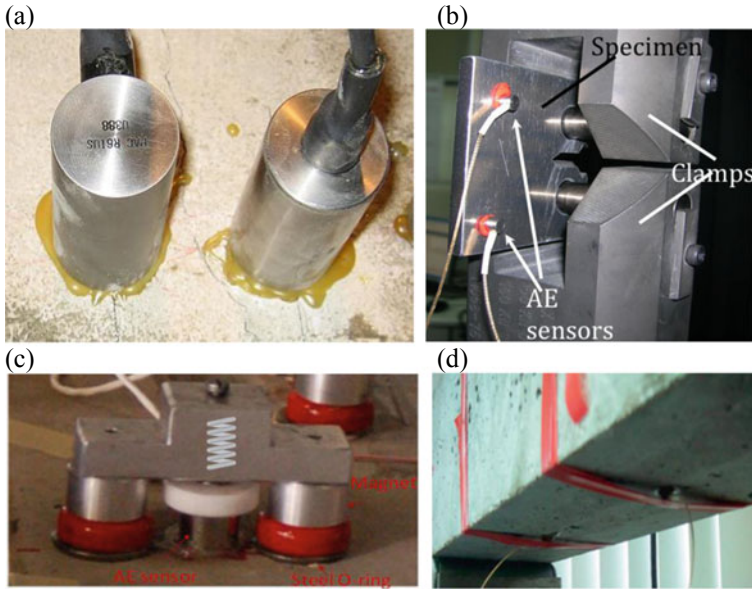


Fig. 14 Mounting of AE sensors: **a, b** with wax on concrete and aluminium respectively, **c** with magnetic clamps, **d** with grease and tape

springs, magnetic hold-downs, and other special fixtures. It is important that any mechanical mount does not make electrical contact between the sensor case and the structure. Accordingly, grounding the case is often necessary. Examples of sensor mounting can be seen in Fig. 14.

Apart from the characteristics of sensor and specifically the piezoelectric element, there is another specific point in the manner the waves are “felt” or acquired by the sensor. Especially, in plate structures the wave direction is predominantly parallel to the sensor face while in a general case of a bulk medium, the AE wave comes at an angle or even close to 90° if the source is deep inside the material. This changes the actual output of the sensor due to the “aperture” effect. Therefore, a sensor sensitivity curve obtained by direct incidence calibration may exhibit strong differences to the corresponding curve when the same excitation is conducted at the same distance but on the surface. The reason is connected to the diameter of the sensor since the exerted voltage is an integration of the response of the whole contact surface or in other words the voltage output is derived from the average disturbance over the whole surface of the element. Therefore, the larger the surface area of a transducer, the higher is the possibility to interfere with the waveform shape, see Fig. 15. When the diameter increases, it becomes possible that many cycles of the wave are simultaneously acting on the sensor surface and their contribution is averaged, something that essentially acts as a cutting off filter for higher frequencies. Any distortions compared to the “point” receiver are treated as a deviation from the ideal behavior. Also known as “aperture” effect, it is demonstrated as a decrease in the recorded wave amplitude at

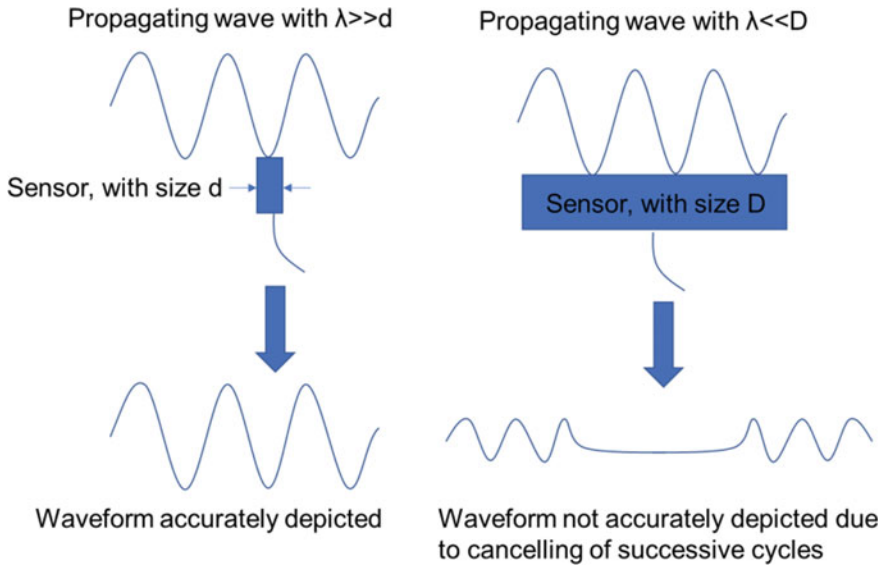


Fig. 15 Schematic representation of sensor size and wavelength influence on the recorded waveform

high frequencies due to multiple wavelengths being averaged over the area of contact of a sensor (McLaskey and Glaser 2012).

The aperture effect on wave propagation has been highlighted in numerical studies, considering the sensor response function on plate geometries (Sause et al. 2012). It was found that for smaller tip size a better match with the reference wave (wave without the presence of the sensor) was observed. In another case, it was seen that the sensor sensitivity curves corresponding to longitudinal, surface, guided and plate waves differ substantially, especially for resonant sensors pointing at the aperture effect (Sause and Hamstad 2018). Therefore, the calibration procedure is reasonable to consider the type of the propagating wave (e.g. for plate wave applications, calibration should be conducted by Lamb waves). Similar conclusions were drawn, comparing the sensitivity curves of different transducers for normal incident wave, versus parallel propagation in the form of guided waves (Ono et al. 2017). It was shown that the sensitivity for normal waves is higher than the response to the other two types of waves. In addition, the sensor with the smallest diameter exhibited the aperture influence (drop of sensitivity for parallel waves compared to normal) at higher frequencies, while the larger sensors exhibited a discrepancy at lower frequencies. The same phenomenon can be seen for Rayleigh waves since the propagation direction is parallel to the sensor surface (Tsangouri and Aggelis 2018).

To illustrate this phenomenon, numerical simulations are very useful. Experimentally, although sensors with different diameter are available, these would also exhibit different resonance and therefore, the effect of size would not be isolated. This is

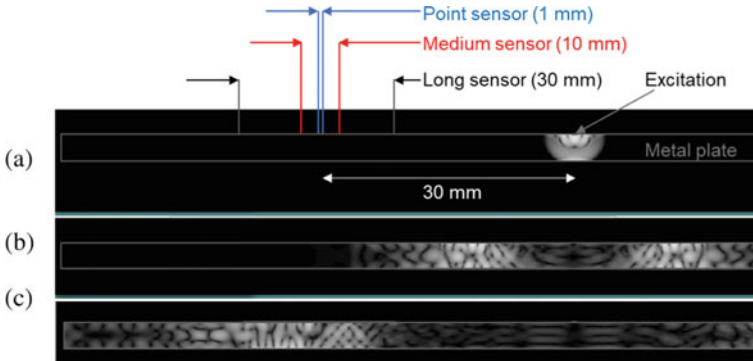


Fig. 16 Snapshots of the transient strain field in a metal plate after three cycles of 1 MHz excitation **a** 1 μ s, **b** 8 μ s, and **c** 10 μ s after the excitation

illustrated by the following indicative simulations using (Wave2000Plus). The geometry is considered a plate with properties close to aluminum ($C_P = 6583$ m/s, $C_S = 3388$ m/s) and thickness of 5 mm (Fig. 16). The point excitation is three cycles of 1 MHz in one case and 100 kHz in a second case with direction vertical to the surface. Three virtual receivers are placed with center-to-center distance of 50 mm from the source. One is 30 mm long, the other 10 mm and the last is a “point” receiver of 1 mm size (see Fig. 16). The resolution in space is 0.2 mm (much smaller than the wavelengths) and the sampling rate is almost 80 MHz (much higher than the applied frequencies). Three snapshots of the strain field at different times after the excitation are given in Fig. 16.

The difference in the waveforms received by the three sensors for the 1 MHz excitation is seen in Fig. 17a. The point sensor exhibits by far the highest amplitude as its whole surface “area” (line in this 2D simulation) is excited by the same phase of the wave. On the other hand, the long sensor of 30 mm, exhibits much smaller amplitude, since even when the maximum pressure of the wave is exciting a part of the sensor, this is averaged along the whole sensor length with other parts of the line sensing less pressure, or even opposite phase. The power spectra in Fig. 17b are also characteristic. The frequency of the excitation seems to survive only on the point receiver which shows most of its content around 1 MHz. This frequency band is very weak for the larger sensors and especially the one with 30 mm size. In this case, the nominal wavelength is approximately 6–7 mm implying that a sensor with much larger size seriously masks the content.

For the second case concerning lower frequency of 100 kHz (and longer wavelength—in this case 60–70 mm) the situation improves in terms of the surviving frequency. Still the point sensor has the highest signal followed by the medium sensor of 10 mm, which exhibits a similar waveform but with 30% reduced amplitude (Fig. 17c). In this case even the large sensor of 30 mm captures the main frequency content showing a clear peak at 100 kHz (see Fig. 17d). This simple 2D simulation is indicative of the influence of the physical size of the transducer in case of plate waves.

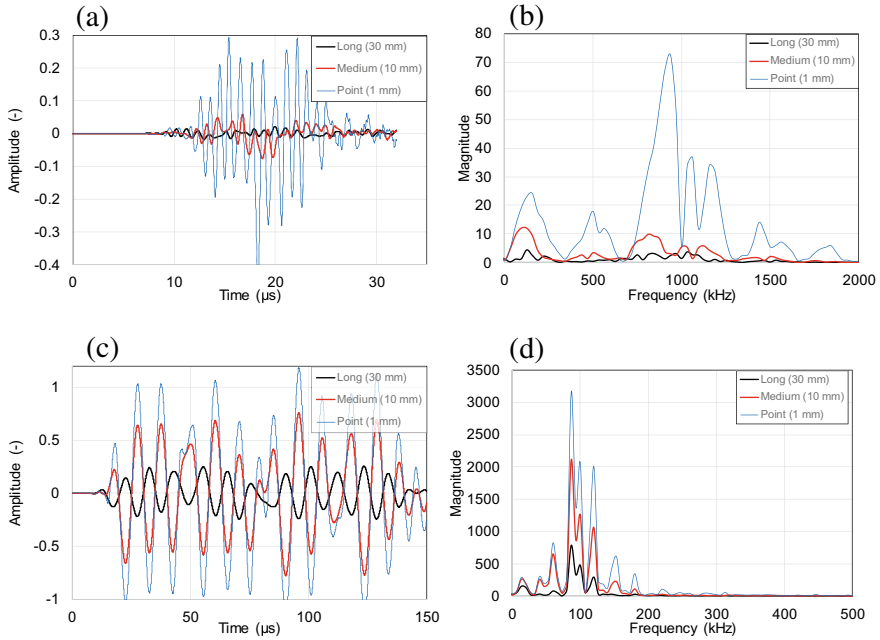


Fig. 17 Simulated waveforms collected on metal specimen by sensors of different size after excitation of **a** 1 MHz, **b** corresponding power spectra, **c** 100 kHz, **d** corresponding power spectra

It is highlighted that, the effect of the size alone is isolated and studied, something that is difficult experimentally as different sizes of sensors will also have different resonant behaviors and piezoelectric conversion factors. The aperture effect is strong for surface propagation in bulk media as well, but weakens for diagonal or vertical propagation, typically occurring in bulk media (Tsangouri and Aggelis 2018).

5 Other Types of Sensors

Besides the PZT sensors, new types of sensors are under development. As discussed before, the laser system has been applied to AE detection. It is a contactless measurement but less sensitive than the PZT sensors. Consequently, it has been applied to AE phenomena of large amplitudes. An example is illustrated in Fig. 18 (Nishinoiri and Enoki 2004). The PZT sensors have a limitation in application at elevated temperature, because PZT has Curie point. In contrast, the laser system is applicable to AE measurement in ceramics under firing. This is because cracking under firing of structural ceramics causes a serious problem for fabrication. Cracks are generated in heating, sintering or cooling, so that AE monitoring was applied to optimize firing conditions.

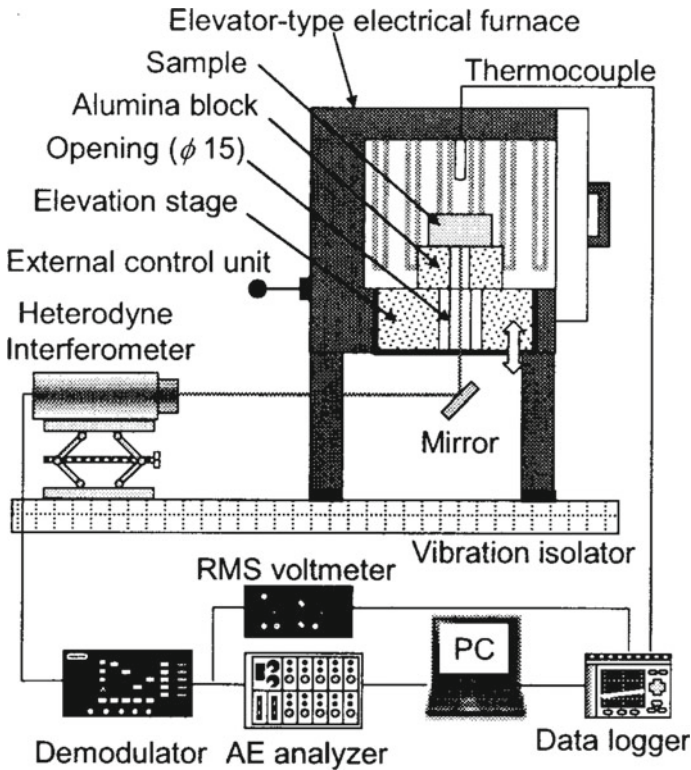


Fig. 18 Laser AE system at high temperature

An optical fiber sensor is a new and an attractive AE sensor as alternative to the PZT sensor. It can offer a number of advantages such as the long-term monitoring, the condition free from electro-magnetic noises, and the use of corrosive and elevated environments. One example applied to a pipe structure is illustrated in Fig. 19 (Cho et al. 2004). According to their results, the sensitivity depends on the number of fiber winding, and is still 10 times lower than a conventional PZT sensor. It is noted that physical quantity of measured AE signals is not confirmed yet. It is expected that radial displacement motions could be associated with AE signals detected.

6 Instrument

AE sensors transform surface motions into electric signals. Thus, the amplifiers are usually employed to magnify AE signals. Because cables from the sensor to the amplifier are subjected to electro-magnetic noise, specially coated cables of short length shall be used. Preamplifiers with state-of-the-art transistors should be used

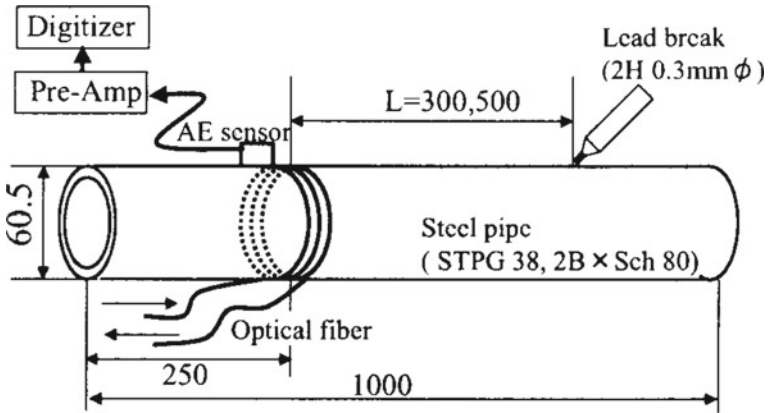


Fig. 19 Fiber-optic AE sensor for a pipe structure

to minimize the amount of electronic noise. Amplifiers with a flat response in the frequency range are best use.

AE signals are normally amplified both by a pre-amplifier and by a main-amplifier and are filtered. The gain of the amplifier is given in dB (decibels), which means the ratio between input voltage V_i and output voltage V_o as,

$$dB = 20 \log_{10}(V_o/V_i). \tag{12}$$

A filter of variable band-width between 1 kHz and 2 MHz is generally employed. The choice of the frequency range depends on noise level and attenuation property of concrete. As given in Fig. 20, it is noted that the use of the band-pass filter drastically changes AE signals.

The attenuation of elastic waves is quantitatively represented by the Q value. When the wave with energy level E is attenuated by ΔE over one-wavelength propagation, Q is defined as,

$$Q = 2\pi E/\Delta E. \tag{13}$$

In the case of a pure elastic material, $\Delta E = 0$ and Q becomes infinite. The larger Q is, the lower the attenuation is. Q is larger than 1000 for typical metals, while Q is reported as lower than 100 in concrete (Ohtsu 1987). When AE waves propagate for distance D , the amplitude $U(f)$ of frequency components f attenuates from U_0 to,

$$U(f) = U_0 \exp(-\pi f D/\nu Q) \tag{14}$$

Substituting frequency $f = 1$ MHz, distance $D = 1$ m, velocity of P-wave $\nu = 4000$ m/s, and $Q = 100$, the attenuation $U(f)/U_0$ becomes -68 dB/m. Thus, the higher frequency components are, the more quickly they attenuate.

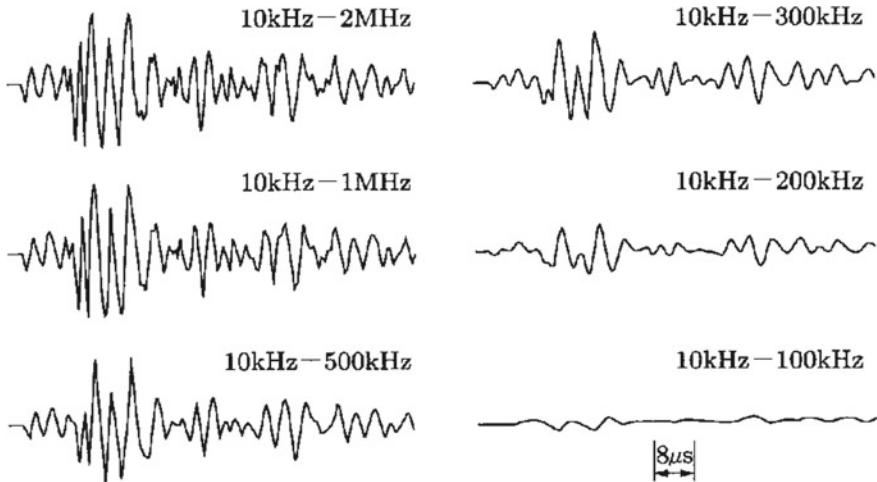


Fig. 20 Effect of the band-pass filter on AE waveforms

7 Data Acquisition and Wave Parameters

Main concern for data acquisition results from the A/D (analog to digital) conversion and the triggering. Fast A/D units have to be used to ensure that a large number of events are recorded. Usually, the A/D converter is equipped for each channel of the recording unit. Anti-aliasing filters are required so that the signals can be properly transformed to the frequency domain. A photograph of an AE instrument is shown in Fig. 21 Signal data are mostly digitized by employing a personal computer system.

A monitoring system can analyze parameters like count, hit, event, rise time, duration, peak amplitude, energy, RMS (root mean square) voltage, frequency spectrum, and arrival-time difference as discussed in chapter “[Parameter based AE analysis](#)”. Normally AE signals are processed after the amplitude becomes larger than the threshold level.

8 Concluding Remarks

Sensors and AE equipments are already commercially available. They are going to be further updated due to evolution of LSI circuits and IoT devices. In this concern, important aspects are to select proper sensors and instrumental systems. Depending upon materials and structures, selection of sensors, decision of frequency range, techniques to eliminate noise and conditions for system setting may change. Some of standardized procedures and requirements for systems are stated in chapters dealing



Fig. 21 One type of multi-channel AE system

with applications. Concerning AE measurement in concrete, one ISO standard is recently published (ISO16836 [2019](#)).

References

- Auld BA (1973) *Acoustic fields and waves in solids*. John Wiley & Sons, New York
- Beattie AG (1983) Acoustic emission, principles and instrumentation. *J Acoust Emiss* 2(1/2):95–128
- Breckenridge FR (1982) Acoustic emission transducer calibration by means of the seismic surface pulse. *J Acoust Emiss* 1(2):87–94
- Cho H, Arai Y, Takemoto M (2004) Development of stabilized and high sensitive optical fiber acoustic emission system and its application. *Progress in AE XII*:43–48, JSNDI
- Godin N, Reynaud P, Fantozzi G (2018) Challenges and limitations in the identification of acoustic emission signature of damage mechanisms in composites materials. *Appl Sci* 8(8), article number 1267
- Hatano H, Watanabe T (1997) Reciprocity calibration of acoustic emission transducers in rayleigh wave and longitudinal wave sound field. *J Acoust Soc Am* 101(3):1450–1455
- Herrmann G (1974) *RD Mindlin and applied mechanics*. Pergamon Press, New York
- Holland R, EerNisse EP (1969) *Design of resonance piezoelectric de-vices*. Res Monogr 56, MIT Press, Cambridge
- Hsu NN, Breckenridge FR (1981) Characterization and calibration of acoustic emission sensors. *Mater Eval* 39:60–68

- ISO16836 (2019) Non-destructive testing—acoustic emission inspection measurement method for acoustic emission signals in concrete
- Kawabata A (1973) Ultrasonic piezoelectric sensors and their application. *J Soc Mater Sci Jpn* 22(232):96–101
- Mason WP (1958) *Physical acoustic and properties of solids*. Princeton, D van Nod-trand Company
- McLaskey GC, Glaser SD (2012) Acoustic emission sensor calibration for absolute source measurements. *J Nondestruct Eval* 1–12
- Nishinoiri S, Enoki M (2004) Development of in-situ monitoring system for sintering of ceramics using laser AE technique. *Progress in AE XII:69–76*, JSNDI
- Ohtsu M, Ono K (1983) Resonance analysis of piezoelectric transducer Elements. *J. Acoust Emiss* 2(4):247–260
- Ohtsu M, Ono K (1984) A generalized theory of acoustic emission and Green's functions in a half space. *J Acoust Emiss* 3(1):124–133
- Ohtsu M (1987) Acoustic emission characteristics in concrete and diagnostic applications. *J Acoiust Emiss* 6(2):99–108
- Ono K, Hayashi T, Cho H (2017) Bar-wave calibration of acoustic emission sensors. *Appl Sci* 7:964
- Papasalouros D, Bollas K, Kourousis D, Anastasopoulos A (2016) Acoustic emission monitoring of high temperature process vessels & reactors during cool down. In: *Emerging technologies in non-destructive testing VI—proceedings of the 6th international conference on emerging technologies in nondestructive testing, ETNDT*, pp 197–201
- Perkeris CL (1955) The seismic surface pulse. *Proc Natl Acad Sci* 41:469–480
- Proctor TM (1982) Some details on the NBS conical transducer. *J. Acoust Emiss* 1(3):173–178
- Sansalone MJ, Streett WB (1997) *Impact-echo*. NY Burier Press, Ithaca
- Sause MGR, Hamstad MA (2018) Numerical modeling of existing acoustic emission sensor absolute calibration approaches. *Sens Actuators Phys* 269:294–307
- Sause MGR, Hamstad MA, Horn S (2012) Finite element modeling of conical acoustic emission sensors and corresponding experiments. *Sens Actuators Phys* 184:64–71
- To AC, Glaser SD (2005) Full waveform inversion of a 3-D source inside an artificial rock. *J Sound Vib* 285:835–857
- Tsangouri E, Aggelis DG (2018) The influence of sensor size on acoustic emission waveforms—a numerical study. *Appl Sci (Switzerland)*, 8(2), art. no. 168
- Wave2000Plus (2020) <https://cyberlogic.org/wave2000plus.html>. Accessed February 2020
- Zelenyak A-M, Hamstad MA, Sause MGR (2015) Modeling of acoustic emission signal propagation in waveguides sensors (Switzerland) 15(5):1805–11822